

Photovoltaic performance of novel push–pull–push thienyl–Bodipy dyes in solution-processed BHJ-solar cells†

Cite this: *New J. Chem.*, 2014, **38**, 1701

Alexandra Sutter,^a Pascal Retailleau,^b Wei-Ching Huang,^c Hao-Wu Lin*^c and Raymond Ziessel*^a

Received (in Montpellier, France)
18th November 2013,
Accepted 5th February 2014

DOI: 10.1039/c3nj01436c

www.rsc.org/njc

This work explores the synthesis of extended dipyrromethene dyes engineered from thiophene-linked triphenylamine modules in order to favor pronounced charge transfer within the dyes and to enable their use in solar cells. We found that these soluble dyes absorb up to 760 nm in solution and 850 nm in thin films. An effective charge transfer absorption band was found at around 460 nm. In the crystal lattice, molecules are organized in layers separated by 3.50 Å with pronounced π – π stacking and S...S interactions. The electroactivity of the dyes indicates that electron injection in PC₇₁BM is feasible. Bulk heterojunction solar cells based upon dyes **1** and **2** in an optimized device structure ITO/Ca/**1** or **2**:PC₇₁BM/MoO₃/Ag provide a power conversion efficiency of about 1.5% after thermal annealing.

1. Introduction

The fabrication of solar energy conversion devices is a major contemporary interest of the general scientific community due to their promise as low-cost and renewable energy sources.¹ Production of organic solar cells (OSCs) by solution-processing techniques is a promising technology for cheap and flexible panels.² Usually the photoactive layer is made of a blend of a small and highly colored organic molecule or a soluble low band-gap polymer considered as the electron donor and a soluble fullerene derivative able to accept the photo-excited electron.³ Note that small molecules can be co-evaporated with the acceptor under ultra-high vacuum to form the photoactive layer. In both cases nanophase-segregation between the donor and the acceptor is mandatory to provide high efficiency.⁴ Impressive photoconversion efficiencies of 8.9%⁵ to above 10%⁶ were recently reached using small molecules and both technological approaches.

A key factor for the success of OSCs is the nature of the dyes which absorb the photons, allow diffusion of the excitons in the thin layer and finally promote charge separation at the interface with the acceptor in the bulk-heterojunction (BHJ).⁷ Many dyes have been screened including oligothiophenes,⁸ diketopyrrolopyrroles (DPP),⁹ mixed DPP-TAT dumbbell-shaped scaffoldings (TAT for triazatruxene),¹⁰ squaraines,¹¹ hexabenzocoronenes,¹² merocyanines,¹³ donor–acceptor oxoindanes,¹⁴ thiadiazolo-bithienyls,¹⁵ benzodithiophenes,¹⁶ benzothia-diazoles,¹⁷ and Bodipy-thienyls.^{18,19}

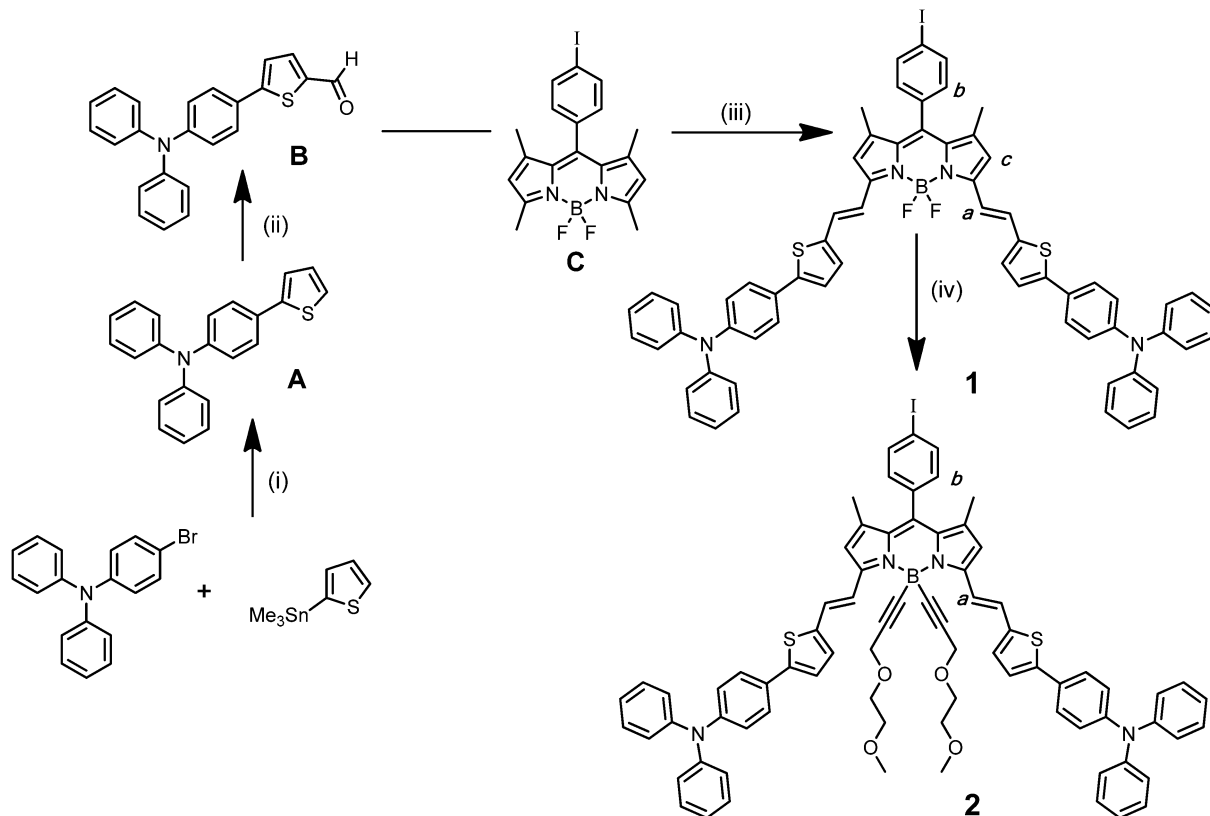
Borondipyrromethene (Bodipy) dyes are attractive for use in organic photovoltaic cells (OPVs)^{18–20} and dye-sensitized solar cells (DSSCs)²¹ mostly because many chemical tools allow tailoring at will of the optical and redox properties.²² Consequently, several substituted Bodipy dyes were tested as sensitizers in BHJ solar cells with photoconversion efficiencies spanning from 0.9 to 4.7%. Some of these Bodipys were constructed with vinyl side arms in the 3,5-substitution positions, ensuring extended delocalization pathways in the ground state and intense absorption in the visible portion of the electromagnetic spectra. In some cases, these vinyl groups were elaborated with strong donor groups like triazatruxene providing good charge transport in the active layer and a good match with the solar spectrum.^{20b} Interestingly, mixing of similar dyes allowed extension of the photon absorptivity of the device and ensured better photon to current conversion.^{18b} The use of thiophene-grafted Bodipys markedly improved the efficiency, mostly due to high mobility of hole and electron inside the thin photoactive layer.¹⁹ It has further been demonstrated that a very high open-circuit voltage could be achieved by linking triphenylamine (TPA) fragments in the 2,6-substitution positions of a Bodipy framework.^{20c}

^a Laboratoire de Chimie Organique et Spectroscopies Avancées (ICPEES-LCOSA), UMR 7515 au CNRS, Ecole Européenne de Chimie, Polymères et Matériaux, Université de Strasbourg, 25 rue Becquerel, 67087 Strasbourg Cedex 02, France. E-mail: ziessel@unistra.fr

^b Centre de Recherche de Gif, Institut de Chimie des Substances Naturelles, UPR2301-CNRS, Bâtiment 27, 1 avenue de la Terrasse, 91198 Gif sur Yvette Cedex, France

^c Department of Materials Science and Engineering, National Tsing Hua University, Hsinchu, Taiwan. E-mail: hwlin@mx.nthu.edu.tw

† Electronic supplementary information (ESI) available. CCDC 939187. For ESI and crystallographic data in CIF or other electronic format see DOI: 10.1039/c3nj01436c



Scheme 1 Keys: (i) [Pd(PPh₃)₄] (6 mol%), toluene, 110 °C, overnight; (ii) (a) POCl₃ (1.1 eq.), DMF (1.4 eq.), 0 °C, 1 h, (b) compound A (1 eq.), 1,2-dichloroethane, 85 °C, overnight; (iii) compound C (1 eq.), compound B (3 eq.), piperidine, *p*-TsOH, toluene, reflux, Dean-Stark apparatus, overnight; (iv) (a) 3-(2-methoxyethoxy)prop-1-yne (4 eq.), EtMgBr (3.5 eq.), THF, 60 °C, 2 h, (b) compound 1 (1 eq.), THF, 60 °C, overnight.

Herein we describe novel extended Bodipy dyes built from both TPA-thiophene (push) modules in a conjugated situation with a 3,5-substituted Bodipy (pull) skeleton. The idea was to increase the electronic density on the thiophene site in order to favour charge transfer with the electron withdrawing Bodipy module without perturbing to a large extent the electrochemical gap (HOMO/LUMO). The target dyes were prepared as shown in Scheme 1. The rationales for the fluorine group substitution rely on our previous work, where we increase the steric bulkiness around the boron center to avoid the aggregation process and increase the solubility and chemical and photochemical stability of the dyes.²³

2 Experimental part

2.1 General methods

All chemicals were obtained from commercial sources (Sigma Aldrich, Alfa Aesar) and used, unless otherwise stated, without further purification. All anhydrous reactions were performed under a dry atmosphere of argon using standard Schlenk techniques. THF was distilled over sodium and benzophenone under an argon atmosphere. 1,2-Dichloroethane was distilled over P₂O₅ under an argon atmosphere. DMF and thiophene were distilled over potassium hydroxide under argon.

¹H NMR, ¹³C NMR and ¹¹B NMR spectra were recorded on BRUKER spectrometers with reference chemical shifts taken as

CHCl₃ ($\delta = 7.26$ ppm) for ¹H NMR, and CDCl₃ ($\delta = 77.2$ ppm) for ¹³C NMR, while the signal from the B within the borosilicate of the NMR tubes was used for ¹¹B NMR. Electronic absorption spectra were recorded using a Shimadzu UV-3600 dual-beam grating spectrophotometer with a 1 cm quartz cell. Steady-state emission and excitation spectra were recorded on a HORIBA Jobin-Yvon FluoroMax 4P spectrofluorimeter. All fluorescence spectra were corrected. The fluorescence quantum yield (Φ_{exp}) was calculated from eqn (1):

$$\Phi_{\text{exp}} = \Phi_{\text{ref}} \frac{F[1 - \exp(-A_{\text{ref}} \ln 10)]n}{F_{\text{ref}}[1 - \exp(-A \ln 10)]n_{\text{ref}}^2} \quad (1)$$

Here, F denotes the integral of the corrected fluorescence spectrum, A is the absorbance at the excitation wavelength and n is the refractive index of the medium.

Tetramethoxydiisoindomethene-difluoroborate ($\phi_{\text{F}} = 0.51$ in dichloromethane) was used as the emission reference for both compounds emitting above 650 nm.²⁴

Potentials are determined by cyclic voltammetry in deoxygenated CH₂Cl₂ solutions, containing 0.1 M TBAPF₆, at a solute concentration range of *ca.* 1 mM and at rt. Potentials are given *versus* the saturated calomel electrode (SCE) and standardized *vs.* ferrocene (Fc) as internal reference assuming that $E_{1/2}(\text{Fc}/\text{Fc}^+) = +0.38$ V ($\Delta E_{\text{p}} = 60$ mV) *vs.* SCE. The error in half-wave potentials is ± 10 mV. Where the redox processes are irreversible, the peak

potentials (E_{ap} or E_{cp}) are quoted. All reversible redox steps result from one-electron processes unless otherwise specified.

2.2 Preparative work

Materials. $[Pd(PPh_3)_4]$,²⁵ **A**,²⁶ **B**,²⁷ Bodipy **C**,^{17,18} and 3-(2-methoxyethoxy)prop-1-yne¹⁸ were synthesized according to the indicated literature procedures. The preparation of trimethyl(thiophen-2-yl)stannane was adapted from ref. 26 by replacing tri-*n*-butylstannylchloride by trimethylstannyl-chloride.

Synthesis of 1. To a solution of Bodipy **C** (199.8 mg, 0.44 mmol) in toluene (40 mL) were added 5-(4-diphenylamino-phenyl)-2-carbaldehydethiophene **B** (473.5 mg, 1.33 mmol), piperidine (1 mL) and one crystal of *p*-toluenesulfonic acid. The resulting mixture was stirred at reflux overnight using a Dean-Stark apparatus. After being cooled, the organic product was extracted into CH_2Cl_2 , and washed with water and brine. The organic layer was dried over anhydrous $MgSO_4$ and evaporated under vacuum. The crude product was purified by silica gel chromatography (from 60/40 to 50/50 petroleum ether/ CH_2Cl_2) and recrystallized by slow evaporation of dichloromethane from a mixture of CH_2Cl_2 -EtOH. The resulting crystals were collected and washed with pentane to afford a green compound (431.1 mg, 86%). ¹H NMR δ (ppm): (300 MHz, $CDCl_3$): δ (ppm) 7.85 (d, ³*J* = 8.1 Hz, 2H), 7.42–7.55 (m, 6H), 7.01–7.36 (m, 32H), 6.60 (s, 2H), 1.47 (s, 6H). ¹³C NMR (300 MHz, $CDCl_3$): δ (ppm) 152.3, 147.8, 147.4, 146.3, 141.3, 140.8, 138.2, 134.9, 133.5, 130.7, 129.4, 129.2, 127.9, 126.7, 124.7, 123.4, 123.3, 123.2, 118.2, 117.7, 94.7, 14.9. EI-MS *m/z* (%) 1124.1 (100). Anal. for $C_{65}H_{48}BF_2IN_4S_2$: found C, 69.31; H, 4.21; N, 4.68; calcd for $C_{65}H_{48}BF_2IN_4S_2$: C, 69.40; H, 4.30; N, 4.98.

Synthesis of 2. In a Schlenk flask, ethylmagnesiumbromide (702.8 μ L, 0.80 mmol) was added to a stirred solution of 3-(2-methoxyethoxy)prop-1-yne (96.3 μ L, 0.70 mmol) in anhydrous THF (5 mL). The mixture was stirred at 60 °C for 2 h under argon. The resulting anion was then transferred with a canula to a solution of **1** (225.9 mg, 0.20 mmol) in anhydrous THF (5 mL). After the reaction mixture was stirred at 60 °C overnight under argon, water was added, and the solution was extracted with CH_2Cl_2 . The organic phase was washed with water, dried over anhydrous $MgSO_4$ and evaporated under vacuum. The crude product was purified by silica gel chromatography (from pure CH_2Cl_2 to 98/2 CH_2Cl_2 /MeOH) and recrystallized by evaporation in CH_2Cl_2 /EtOH to afford a green compound **2** (198.2 mg, 75%) after washing with pentane. ¹H NMR (300 MHz, $CDCl_3$) δ (ppm): 8.00 (d, ³*J* = 15.9 Hz, 2H), 7.85 (d, *J* = 8.3 Hz, 2H), 7.52 (d, ³*J* = 8.6 Hz, 4H), 6.98–7.33 (m, 32H), 6.61 (s, 2H), 4.23 (s, 4H), 3.64–3.71 (m, 4H), 3.28–3.35 (m, 4H), 3.16 (s, 6H), 1.45 (s, 6H). ¹³C NMR (300 MHz, $CDCl_3$) δ (ppm) 151.5, 147.8, 147.2, 145.9, 141.5, 139.9, 138.2, 136.1, 135.24, 131.8, 130.8, 129.4, 127.8, 127.3, 126.7, 124.7, 123.4, 119.7, 118.5, 71.7, 68.3, 59.4, 58.8, 15.1. EI-MS *m/z* (%): 1312.2 (100). Anal. for $C_{77}H_{66}BIN_4O_4S_2$: found C, 70.22; H, 4.86; N, 4.01; calcd for $C_{77}H_{66}BIN_4O_4S_2$: C, 70.42; H, 5.07; N, 4.27.

2.3 Crystallographic section

The structure presented herein was solved from a dark blue single crystal suitable for X-ray diffraction and obtained by slow diffusion of ethanol into a saturated dichloromethane solution

of compound **1**, at room temperature. Diffraction data were collected using a Rigaku MM007 HF copper rotating-anode generator with Osmic confocal optics and a rapid II Curved Image Plate at low temperature, 193 K. A total of 173 images with 5° rotation per image and two minute exposure per degree of oscillation were measured according to an ω -scan profile data strategy derived by the CrystalClear software package.²⁸ Intensities were integrated using FS_Process as implemented in the CrystalClear suite, then corrected for Lorentz-polarization effects, and scaled using symmetry-equivalent reflections using FS_Abscor. The structure was solved by direct methods (SHELXS-97)²⁹ and refined on F2 by means of full-matrix least-squares methods (SHELXL-97).²⁴ All non-hydrogen atoms were allowed anisotropic thermal motion. Aliphatic and aromatic C–H hydrogen atoms were included at calculated positions, with C–H = 0.98 Å, and 0.95 Å respectively and were refined with a riding model and with Uiso set to 1.5 (resp. 1.2) times that of the attached C atom. The structure showed the presence of three disordered dichloromethane solvent molecules with refined occupancy factors less than one but the overall modelling was not satisfactory, requiring resort to the SQUEEZE procedure of Spek and van der Sluis.³⁰ An extra 229 e per cell were indicated, corresponding to 2.7 molecules of CH_2Cl_2 . Their contribution to the diffraction pattern was removed and modified Fo2 written to a new HKL file. The number of electrons thus located was included in the formula, formula weight, calculated density, μ and $F(000)$. ORTEP drawings were made using ORTEP-III³¹ as implemented within PLATON²⁹ and packing studies were carried out using MERCURY.³²

The crystallographic data† are summarized as follows: a dark blue prism of dimensions 0.44 × 0.18 × 0.12 mm, $C_{65}H_{48}BF_2N_4S_2$, 2.7 (CH_2Cl_2), $M = 1354.20$, triclinic, space group *P*-1, $a = 12.6116$ (5), $b = 13.0839$ (6), $c = 20.2570$ (14) Å, $\alpha = 80.833(6)^\circ$, $\beta = 77.449(6)^\circ$, $\gamma = 80.043(6)^\circ$, $V = 3187.7(3)$ Å³, $Z = 2$, $D_{calcd} = 1.411$ g cm⁻³, $F(000) = 1375$, $\mu = 7.039$ mm⁻¹, 14 957 collected reflections ($2.25^\circ \leq \theta \leq 45^\circ$), $-10 \leq h \leq 11$, $-12 \leq k \leq 12$, $-18 \leq l \leq 18$, 22 781 independent reflections ($R_{int} = 0.0481$), goodness-of-fit on F^2 : $S = 1.188$, $R_1 = 0.089$ and $wR_2 = 0.209$ for all 5140 reflections, $R_1 = 0.059$ and $wR_2 = 0.168$ for 5141 observed reflections [$I > 2\sigma(I)$], refining 676 parameters and 41 rigid-bond restraints (DELU with default esd), semi-empirical absorption correction from multi w -scans ($T_{min} = 0.20$, $T_{max} = 0.46$), final electron density between -0.386 and 0.418 eÅ⁻³.

2.4 Device preparation

The OPV devices were fabricated on indium tin oxide (ITO) coated glass substrates (sheet resistance ~ 10 Ω sq⁻¹). The substrates were cleaned in an ultrasonic bath with de-ionized water, acetone, and methanol for 15 min, respectively. The 1 nm Ca layers were deposited onto ITO glass substrates in a high vacuum chamber with a base pressure of $\sim 8 \times 10^{-7}$ Torr, and the deposition was performed at a rate of 1 to 2 Å s⁻¹ with the substrates held at room temperature. A blend solution of solar active Bodipy donors and PC₇₁BM (purchased from Nano-C) was prepared using chloroform as solvent with different ratios and a total concentration of 15 mg mL⁻¹. The active layers were spin-coated on the substrates

in a glove box under an anhydrous nitrogen atmosphere. The samples were then transferred to a vacuum chamber for top electrode deposition. Devices were encapsulated using a UV-cured sealant (Everwide Chemical Co., Epowide EX) and a cover glass under the anhydrous nitrogen atmosphere after fabrication and were measured in air. The active area of the cells had an average size of 5 mm² (intersect area between the Ag cathode and the ITO anode) and was carefully measured device-by-device using a calibrated optical microscope.

2.5 Characteristics measurement

Current density–voltage characteristics were measured using a SourceMeter Keithley 2400 under AM 1.5G simulated solar illumination from a xenon lamp solar simulator (Abet Technologies). The incident light intensity was calibrated as 100 mW cm⁻² using a NREL-traceable KG5 filtered Si reference cell. The external quantum efficiency (EQE) spectra were taken by illuminating chopped monochromatic light with a continuous-wave bias white light (from halogen lamp, intensity ~100 mW cm⁻²) on the solar cells. The photocurrent signals were extracted using a lock-in technique using a current preamplifier (Stanford Research System) followed by a lock-in amplifier (AMETEK). The EQE measurement is fully computer controlled and the intensity of monochromatic light is carefully calibrated using an NIST-traceable optical power meter (Ophir Optronics). Thicknesses and extinction coefficients (*k*) of the thin films were determined using spectroscopic ellipsometry (J. A. Woollam Inc. V-VASE). Atomic force microscopy (AFM) images were taken using a Veeco Nanoscope 3100 atomic force microscope. The electron and hole mobilities for the Bodipy:PC71BM blended films were carried out by using the SCLC method. The hole only device was configured as follows: ITO/MoO₃ (1 nm)/Bodipy:PC₇₁BM (80 nm)/MoO₃ (10 nm)/Al (80 nm), while the electron only device was configured as follows: ITO/Mg (5 nm)/Bodipy:PC₇₁BM (80 nm)/Ca (5 nm)/Al (80 nm). Current density–voltage characteristics of SCLC devices were also measured using a SourceMeter Keithley 2400. The annealing process was performed by placing the encapsulated devices on a temperature controlled hot plate.

3 Results and discussion

3.1 Synthesis and characterization

The synthetic protocol used to prepare the novel dyes is sketched in Scheme 1. The first step produced compound **A** by cross-coupling of 4-(bromophenyl)diphenylamine and 2-trimethyltinthiophene. Formylation of **A** under Vilsmeier–Haack conditions provided regio-selectively the aldehyde **B** in excellent yield under mild conditions. Next, a Knoevenagel reaction using forcing conditions provided the deep-green divinyl derivative **1** in an average yield of 86%. The use of the Grignard reagent of 3-(2-methoxyethoxy)prop-1-yne provided dye **2** in about 75%. All compounds were purified by column chromatography. The molecular structures were assigned by NMR spectroscopy, elemental analysis and mass spectroscopy and these data unambiguously confirm those assigned.

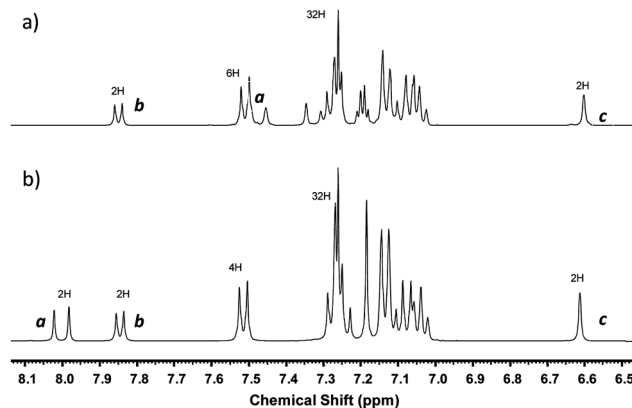


Fig. 1 Partial ¹H NMR spectra of dye **1** (a) and dye **2** (b) in CDCl₃ at rt.

Proton NMR spectra were diagnostic for the state of boron substitution. It has been clearly established that by boron substitution with an ethynyl residue the vinyl protons **a** (2H) at 8.02 ppm ($J_{H-H} = 16$ Hz) are deshielded in **2** by 0.54 ppm, compared to the same protons at 7.48 ppm in the BF₂ compound **1**. In contrast, the doublet at 7.86 ppm (2H, $J_{H-H} = 8$ Hz) assigned to the AB quartet of the phenyl proton **b** in the pseudo *meso* position remained unchanged in both compounds (Fig. 1). Furthermore, the high coupling constants ($J_{H-H} = 16$ Hz) for the vinylic protons are in keeping with a *trans* conformation of the double bonds. Finally, the β-pyrrolic protons **c** remain unchanged at 6.6 ppm.

3.2 X-ray characterization

X-ray diffraction on a blue single crystal confirms that the structure of compound **1** shown in Fig. 2 incorporates a nearly flat 3,5-vinylbisthienyl-Bodipy framework as recently described elsewhere¹⁹ in a related compound (see Fig. 3): it features an even more nearly-planar Bodipy platform (maximum deviation from the mean least-squares plane is 0.107 (8) Å for the carbon

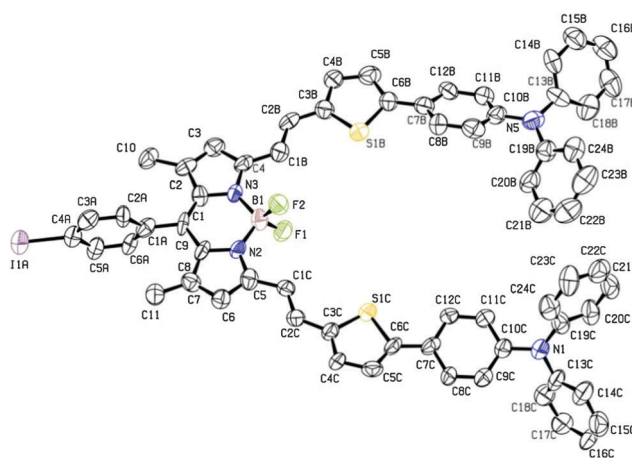


Fig. 2 ORTEP view of compound **1**. Thermal ellipsoids are plotted at the 30% level. B1–N3, B1–N2, B1–F1, B1–F2, N3–C1, N2–C8, N3–C4 and N2–C5 bond lengths are 1.525(14), 1.516(14), 1.376(14), 1.389(13), 1.370(10), 1.370(10), 1.349(11) and 1.368(11) Å, respectively and the FB–F, N–B–F, and N–B–N angles are 107.2(10), 111.0(11)/110.9(11)/110.6(10)/109.2(10) and 107.9(10)°.

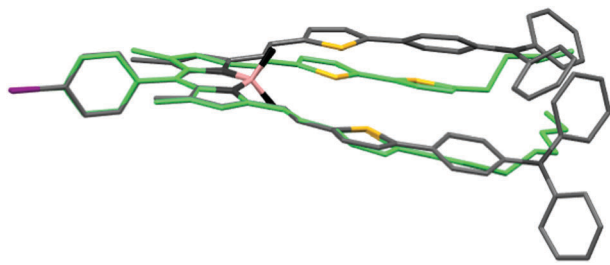


Fig. 3 A superposition of compound **1** and compound 3,5-vinylbisthienyl-Bodipy¹⁸ (in green) generated by least-squares fitting of their iodophenyl-Bodipy groups.

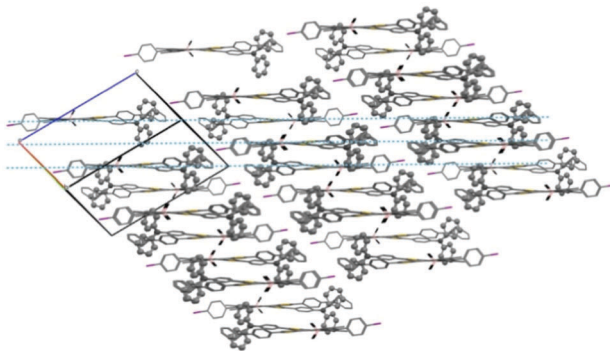


Fig. 4 Lattice view highlighting the layered structure parallel to the (3 3 -4) plane (cyan dotted lines). Phenyl units from the triphenylamine substituents interspersed between the layers are shown as balls.

atom C5) and a near-orthogonally-attached (89.0°) iodobenzene group with $\angle C9 B1 I1$ of 4.2° .

Similarity extends to the sulphur atoms from the first thiophene groups of both arms, which face one another. In the crystal, the flat molecules assemble in a layered structure, parallel to the plane (3 3 -4) with an interplanar separation of $3.50 \pm 0.06 \text{ \AA}$ (Fig. 4). Within a layer, the V-shaped molecules are aligned along the [1 0 -1] direction with the iodophenyl group pointing here towards a phenyl from the triphenylamine unit of one of the two arms, unlike the former complex crystal structure in which the iodobenzene group was inserted between the arms of a neighbor, interacting with the BF_2 group. As a direct consequence, this interaction maintains the thiophene and the phenyl ring bonded to it coplanar with Bodipy platform whereas the other arm is tilted from the mean plane by an angle of circa 9.5° . The triphenylamine unit in interaction with the iodo atom adopts a close to staggered conformation with respect to the mean plane, with the outer phenyl groups interposed between molecular layers. This contrasts with the other triphenylamine unit, where with the phenyl groups are oriented in an eclipsed way. Relative to the mean plane defined by the N atom and its three bound C atoms, the torsion angles of each of the aromatic rings range from 28.6 to 43.3° for the latter group and from 38.6 to 45.0° for the former one, but are similar to the values observed for the diphenylaminophenyl units, $37.0 (7) \leq 50.5 (7)^\circ$.³³ Between adjacent layers, inversion related molecules at general position and at $2 - x$, $1 - y$, $1 - z$ lie pairwise head-to-tail, the Bodipy platform lying over the inside phenyl of the 'flat', eclipsed triphenylamine unit, with the

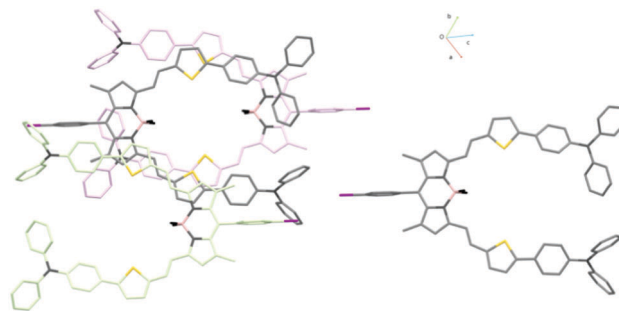


Fig. 5 Part of the crystal structure viewed down the molecular stacking direction. Molecules from $n - 1$, n and $n + 1$ layers are in pink, grey and light green respectively.

arms overlapped and an S...S distance of 4.03 \AA . As well, π - π stacking interactions occur where the molecules at $1 - x$, $1 - y$, $1 - z$ and $2 - x$, $-y$, $1 - z$ in one layer extend one arm towards their equivalent molecule in the next layer, resulting in thiophene groups overlapping the outer five-membered ring of the Bodipy with a centroid-centroid distance of $3.69 \pm 0.03 \text{ \AA}$ (Fig. 5).

3.3 Spectroscopic characterization

Dyes **1** and **2** display similar spectroscopic features (Fig. 6) in THF, with three intense absorption peaks in the 350–550 nm and 600–750 nm range and extinction coefficients of about $70\,000 \text{ M}^{-1} \text{ cm}^{-1}$ for the former peaks and $90\,000 \text{ M}^{-1} \text{ cm}^{-1}$ for

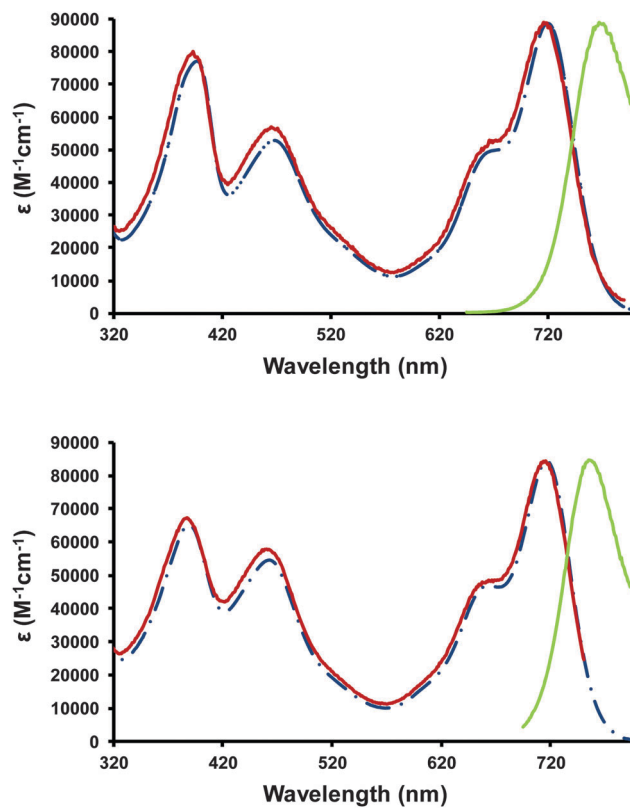


Fig. 6 Absorption (blue trace), emission (green trace) and excitation spectra (red traces) of dye **1** at λ_{exc} @ 640 nm and λ_{em} @ 800 nm (a) and dye **2** (b) at λ_{exc} @ 650 nm and λ_{em} @ 780 nm in THF, at rt.

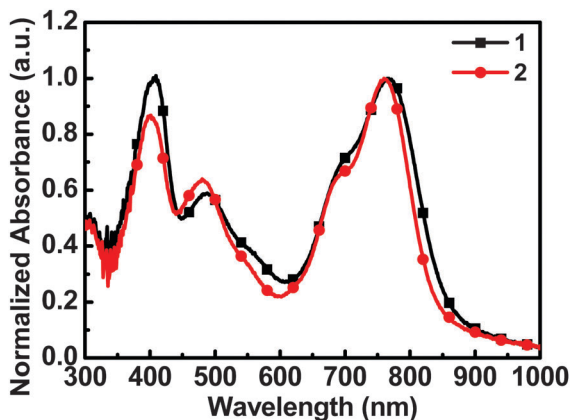


Fig. 7 Thin-film absorption spectra of **1** and **2**.

the latter. The higher energy transition at 391 nm is due to the styryl fragments,³⁴ while that at 719 nm is the $S_0 \rightarrow S_1$ transition of the Bodipy core with a clear vibronic sequence ($\Delta\nu = 1100 \text{ cm}^{-1}$) characteristic of the dipyrromethene framework. The unusual transition observed at 462 nm is not present in most of the styryl derivatives,³⁴ but present when dimethyl-amino residues are used for the construction of the dye, and has been assigned to a charge transfer transition.³⁵ Weak fluorescence at 767 nm for **1** and 758 nm for **2** was detected with an estimated quantum yield of around 3 to 4%. This fluorescence is

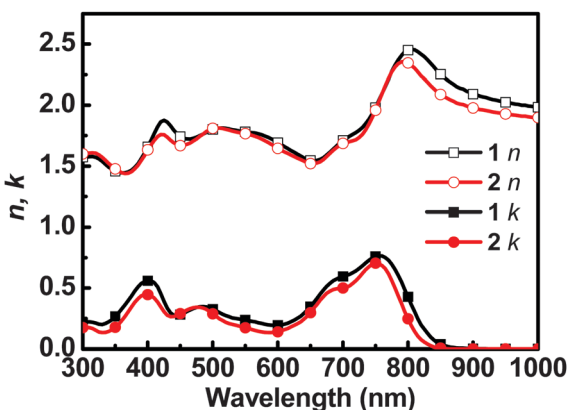


Fig. 8 Optical constants (refractive index, n , and extinction coefficient, k) of **1** and **2** thin films.

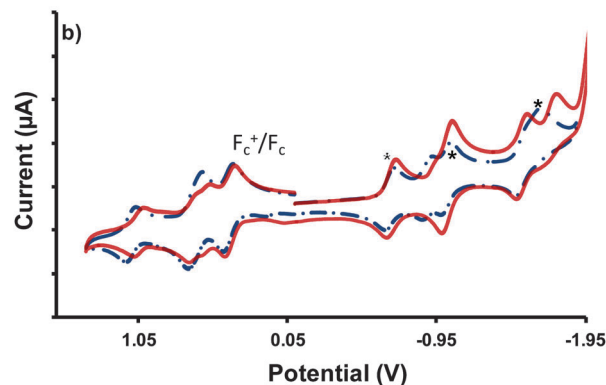
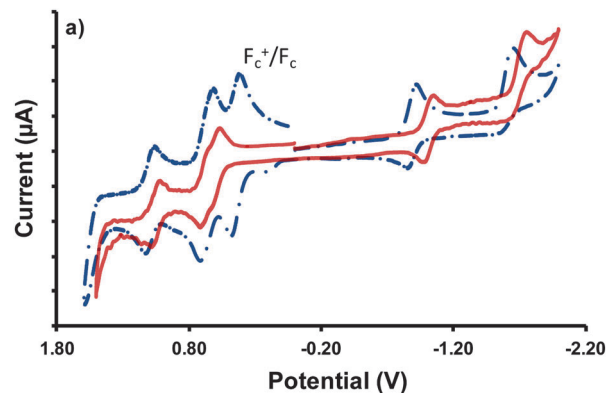


Fig. 9 Cyclic voltammetry of: (a) dye **1** with ferrocene at 0.38 V (blue dashed line) and **2** (red continuous line); (b) dye **1** calibrated with ferrocene and PC₆₁BM (blue dashed line) and **2** with ferrocene and PC₆₁BM (red continuous line). Fc accounts for ferrocene and * for PC₆₁BM.

independent of the excitation wavelength and in both cases the excitation spectra perfectly match the absorption spectra, excluding the presence of aggregates (Fig. 6). The thin-film (thickness of about 50 nm) absorption spectra of **1** and **2** exhibit red-shifts, with $\lambda_{\text{max}} = 766 \text{ nm}$ and 760 nm , respectively (Fig. 7). The red-shift and broadened absorption is possibly due to the π - π interaction in the solid state as seen in the crystal packing. The broad thin-film absorption of **1** and **2** which covers the photo-harvesting range from UV to near-IR is promising for application in photovoltaic devices. Optical constants for **1** and **2** thin films are shown in Fig. 8. The extinction coefficients, k , are consistent with the absorption spectra with high values from 300 nm to 800 nm.

Table 1 Electrochemical data for relevant compounds^a

Dyes	$E^{01}(\text{ox, soln})$ (V), ΔE (mV)	$E^{01}(\text{red, soln})$ (V), ΔE (mV)	Electro-gap (eV)	Optical-gap ^b (eV)
1	+0.59 (70), +1.03 (70)	-0.96 (70), -1.73 (irr.)	1.55	1.58
1 + PCBM*	+0.59 (70), +1.03 (70)	-0.70 (60)*, -0.96 (70)*, -1.08 (70), -1.59 (70)*, -1.80 (irr.)	—	—
2	+0.54 (60), +0.62 (70), +0.99 (60),	-1.07 (60), -1.80 (irr.)	1.61	1.62
2 + PCBM*	+0.54 (60), +0.62 (70), +0.99 (60),	-0.70 (60)*, -0.95 (70)*, -1.07 (60), -1.58 (70)*, -1.78 (irr.)	—	—

^a Potentials determined by cyclic voltammetry in deoxygenated dichloromethane solution, containing 0.1 M TBAPF₆, [electrochemical window from +1.7 to -2.2 V], at a solute concentration of ca. 1.5 mM and at rt. Potentials were standardized versus ferrocene (Fc) as internal reference and converted to the SCE scale assuming that $E_{1/2}(\text{Fc}/\text{Fc}^+) = +0.38 \text{ V}$ ($\Delta E_p = 60 \text{ mV}$) vs. SCE. Error in half-wave potentials is $\pm 10 \text{ mV}$. For irreversible processes the peak potentials (E_{ap}) are quoted. ^b Determined from the absorption spectra from the onset with the tangent at the low energy side.

3.4 Redox properties

Cyclic voltammetry was used to determine the HOMO/LUMO levels of the dyes in solution, with PC₆₁BM and ferrocene used as calibrants. Ferrocene is used because its Fermi level in the vacuum is well-known and PC₆₁BM because this acceptor is used in the real solar cell device. Owing to the low solubility of PC₇₁BM in dichloromethane, PC₆₁BM was preferred for the calibration. Under similar conditions but at low concentration (about 10⁻⁴ M) and at 40 °C, PC₇₁BM is easier to reduce than PC₆₁BM by 120 mV. Both dyes display a rich electrochemistry induced by the presence of various electroactive modules (Table 1, Fig. 9). For both dyes, two reversible oxidation waves at about +0.60 V and +1.00 V were observed. The first of these waves is dielectronic whereas the second process is mono-electronic. No splitting of the waves was observed for dye 1 whereas for the more bulky dye 2 the first oxidation wave was clearly split into two waves at +0.54 and +0.62 V (Fig. 9a). In light of previous electrochemical studies achieved with similar thienyl-derivatives (**D** and **E** in Chart 1) engineered from styryl-derivatives, it clearly appeared that the first oxidative redox potential is assigned to one pyrrole-vinyl-thiophene arm while the second potential (usual similar or very close to the first potential) is assigned to the second pyrrole-vinyl-thiophene arm. In the case of dissymmetric side-arms (*e.g.* **F** in Chart 1), two distinguish potentials are clearly observed.^{19,36} We have previously observed that the shifts of these redox potentials reflect the differing degrees to which the principal donor couples to the extended Bodipy unit.³⁷ DFT calculations indicate that both HOMO and HOMO(-1) are spread over much of the molecule and include contributions from the Bodipy and donor residues. As such, it is inaccurate to ascribe

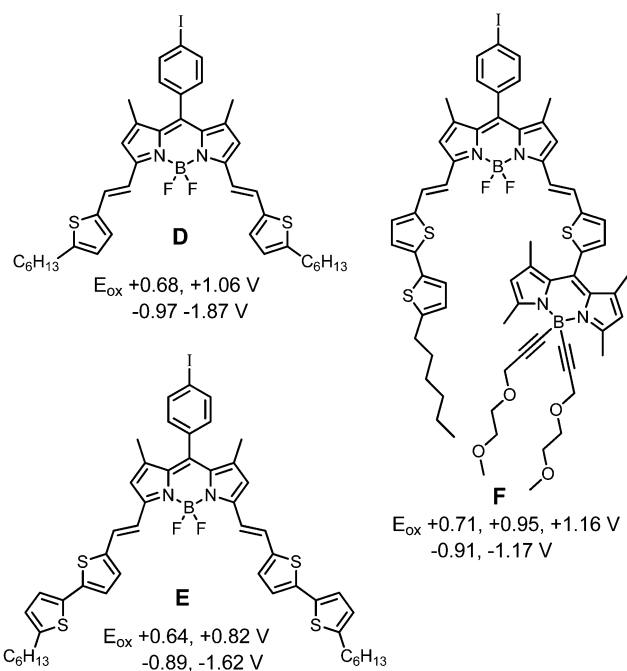


Chart 1 Various thienyl-Bodipy derivatives extracted from ref. 18 (for **D** and **E**) and 35 (for **F**).

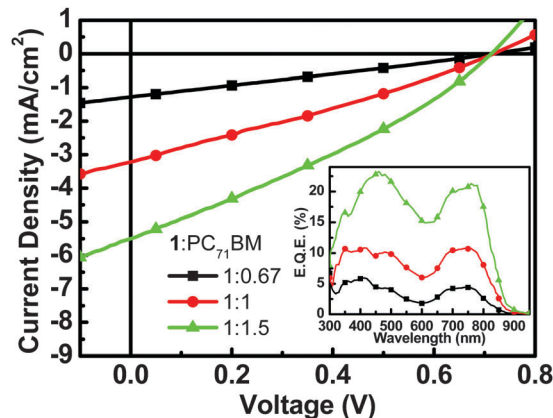


Fig. 10 Current density–voltage characteristics (under AM 1.5G, 100 mW cm⁻² illumination) and EQE spectra (inset) of the 1:PC₇₁BM devices.

Table 2 Performance parameters of devices

Device	V_{OC} (V)	J_{SC} (mA cm ⁻²)	FF	PCE (%)
1:PC ₇₁ BM (1:0.67)	0.72	1.3	0.26	0.24
1:PC ₇₁ BM (1:1)	0.72	3.2	0.28	0.65
1:PC ₇₁ BM (1:1.5)	0.71	5.5	0.31	1.2
2:PC ₇₁ BM (1:0.67)	0.68	3.0	0.30	0.61
2:PC ₇₁ BM (1:1)	0.62	4.3	0.32	0.85
2:PC ₇₁ BM (1:1.5)	0.56	5.5	0.29	0.89
1:PC ₇₁ BM (1:1.5) ^a	0.72	5.5	0.29	1.1
2:PC ₇₁ BM (1:1.5) ^a	0.51	8.9	0.34	1.5

^a 150 °C annealing for 10 min.

the first oxidation step as being localized on either the TPA or the Bodipy unit.

In both cases, two reduction waves were observed at around -1.00 V typical of radical anion formation on the Bodipy core and a second irreversible wave observed at around -1.70 V was assigned to the Bodipy dianion.³⁸ Interestingly, when compared with related dyes *e.g.* 3,5-vinylbisthienyl-Bodipy **B**¹⁹ and as would be expected by the fact that the TPA fragment imports

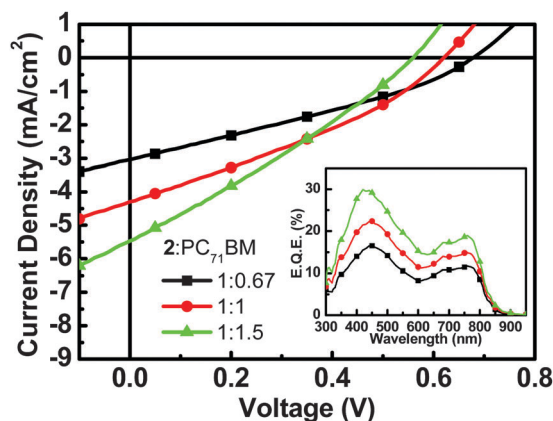


Fig. 11 Current density–voltage characteristics (under AM 1.5G, 100 mW cm⁻² illumination) and EQE spectra (inset) of the 2:PC₇₁BM devices.

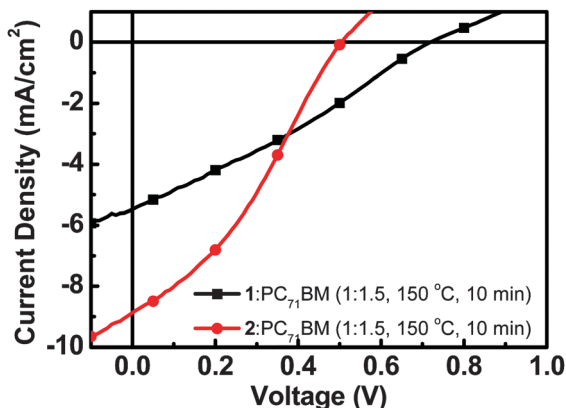


Fig. 12 Current density–voltage characteristics of the 1:PC₇₁BM and 2:PC₇₁BM devices after annealing for 10 min at 150 °C.

additional electronic density, the first oxidation potential in the novel dyes was anodically shifted (easier oxidation) by 50 and 100 mV respectively for **1** and **2**. Whereas, the reduction potentials were anodically shifted (more difficult reduction) by 70 mV and 180 mV respectively for **1** and **2**. Note that there is a significant driving force (about 0.25 eV) for photo-induced electron transfer from the photoexcited dyes toward

PC₆₁BM (Fig. 9b). With the exception of the last reduction potential, all redox processes were highly reversible ($i_{pa}/i_{pc} \approx 1$) and exhibited the characteristic shape ($\Delta E_p = 60\text{--}70$ mV) of a Nernstian process.

3.5 Solar cells and characterization

Ultraviolet photoelectron spectroscopy in air was utilized to measure the energy levels of **1** and **2** in the thin-film state (Fig. S1, ESI†). The HOMO levels of **1** and **2** were found to be -5.14 eV and -5.02 eV, respectively. These values together with the HOMO–LUMO gap estimated from the absorption spectra were used to acquire the LUMO levels of the compounds (-3.50 eV for **1** and -3.37 eV for **2**). The LUMO levels of these compounds are at least 0.2 eV higher than those of fullerenes (-3.7 to -4.3 eV), ensuring efficient charge transfer between **1** and **2** with fullerenes under irradiation.

For photovoltaic characterization, we adopted the inverted structure utilizing ultra-thin 1 nm Ca as a cathode and MoO₃ as a hole extraction layer. The structure has been used in our previous Bodipy cells and showed promising performance.^{20c} The optimized device structure was configured as follows: ITO/Ca (1 nm)/**1** or 2:PC₇₁BM (~ 80 nm)/MoO₃ (7 nm)/Ag (150 nm). The details of optimization are provided in the experimental part. The active layers of the devices were spin-cast from a

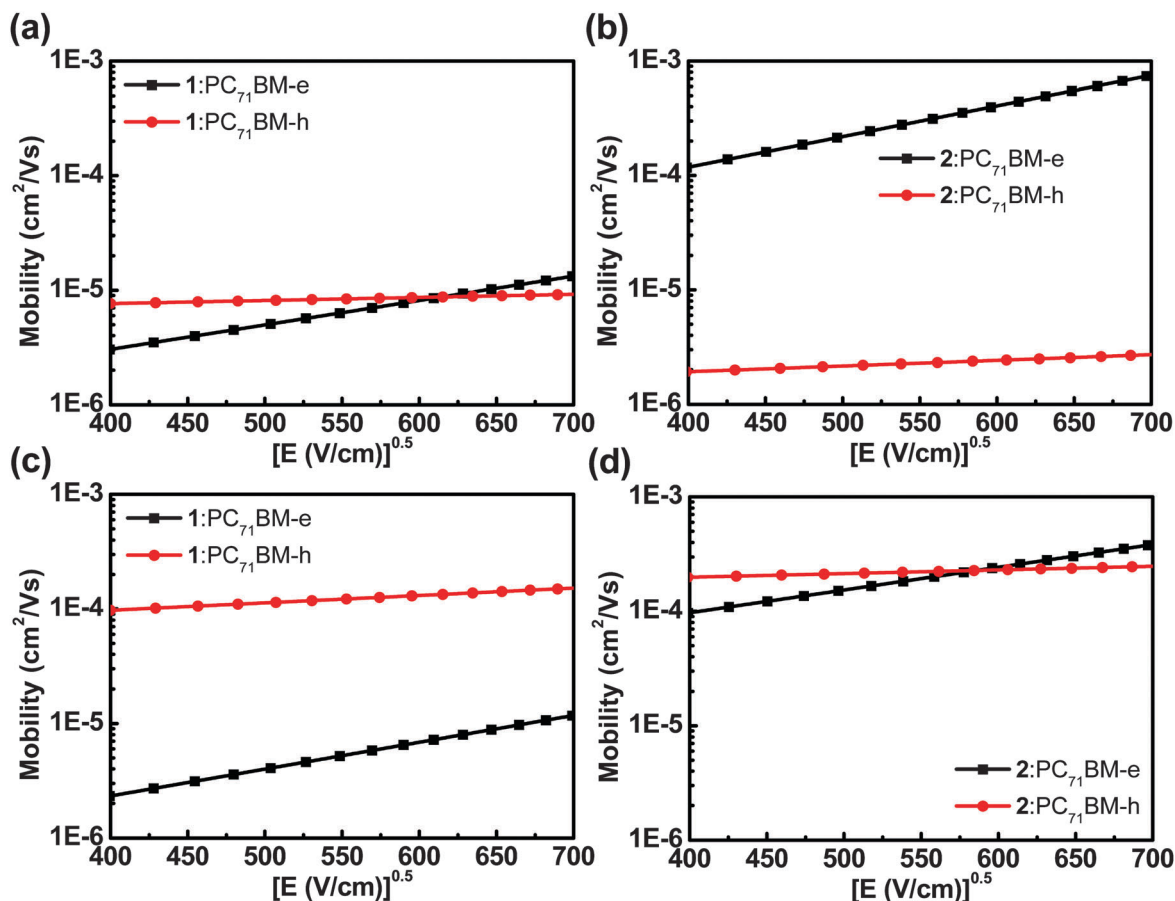


Fig. 13 Carrier mobility of (a) 1:PC₇₁BM, (b) 2:PC₇₁BM BHJ without annealing and (c) 1:PC₇₁BM, (d) 2:PC₇₁BM BHJ after annealing for 10 min at 150 °C.

chloroform solution of the mixture of Bodipy dyes and PC₇₁BM. Fig. 10 shows the current density to voltage (J - V) characteristics and the corresponding external quantum efficiencies (EQEs) of the 1:PC₇₁BM cells. There is negligible difference in the V_{oc} value in the cells with various donor to acceptor ratios (Table 2). However, the J_{sc} and EQE values increased significantly with the increase of the PC₇₁BM ratio. The best cell with 1:PC₇₁BM = 1:1.5 showed a V_{oc} of 0.71 V, a J_{sc} of 5.5 mA cm⁻², a fill factor (FF) of 0.31 and an overall PCE of 1.2%. Fig. 11 shows the J - V and EQE characteristics of the 2:PC₇₁BM cells. The V_{oc} , FF and PCE are lower than that of 1:PC₇₁BM devices. However, as shown in Fig. 12, interestingly, upon annealing the devices at 150 °C for 10 min, the 1:PC₇₁BM cell showed no difference from the device without annealing, but J_{sc} and PCE were considerably increased in the 2:PC₇₁BM devices. This can be rationalized by the carrier mobility in the active layers. The carrier transportation properties were investigated using the space-charge-limited-current (SCLC) method. As shown in Fig. 13, the hole mobilities in the BHJ were all increased after annealing. In the 2:PC₇₁BM thin film, the electron and hole mobilities were initially very unbalanced. Nevertheless, after thermal annealing, the hole mobility was enhanced by 2 orders of magnitude and matched the mobility of electrons. On the other hand, the 1:PC₇₁BM thin film exhibited balanced mobilities without thermal annealing. This may explain why the performance of the 2:PC₇₁BM devices increased upon annealing while that of the 1:PC₇₁BM cell remained constant.

4 Conclusions

In short, we have synthesized new green Bodipy dyes incorporating two thienyl-vinyl units bridging a Bodipy core with two 4-diphenyl-amino-phenyl fragments at the wings. This is an original strategy which does not require post-functionalization of the dyes. The X-ray structure of one of these dyes shows that the main part of the molecule is flat but that its iodophenyl substituent ring is quasi orthogonal (89°) with the main core and that the molecules pack into layers 3.5 Å apart involving π - π and S...S interactions. In the electronic absorption spectra, a new charge transfer band appears at around 460 nm due to interaction between the strong "push" units at the periphery and the central Bodipy "pull" unit. This is an interesting approach which also contributes to the increase of photon absorption either in solution or in the thin film. This strong absorption and redox activity of these dyes enable the preparation of bulk heterojunction with thin films blended with PC₇₁BM which produce a photocurrent reflecting the absorption of the dye in the films. Promising efficiencies at around 1.5% were obtained. We note that the synthetic routes outlined here provide the scope to further tune the performance of the solar cells by postfunctionalization of the phenyl-iodo moiety with electron attractor modules or substituents suitable to promote supramolecular interactions with the electron acceptor.

Acknowledgements

We thank the Centre National de la Recherche Scientifique (CNRS) and National Science Council of Taiwan

(NSC-102-2221-E-007-125-MY3, NSC-101-2112-M-007-017-MY3) for financial support of this work. Professor Jack Harrowfield (ISIS in Strasbourg) is warmly acknowledged for a critical reading of this manuscript prior to publication.

Notes and references

- (a) N. S. Lewis and D. G. Nocera, *Proc. Natl. Acad. Sci. U. S. A.*, 2006, **103**, 15729–15735; (b) N. Armaroli and V. Balzani, *Angew. Chem., Int. Ed.*, 2007, **46**, 52–66; (c) J. Liu, G. Cao, Z. Yang, D. Wang, D. Dubois, X. Zhou, G. L. Graff, L. R. Pederson and J.-G. Zhang, *ChemSusChem*, 2008, **1**, 676–697.
- Organic Photovoltaics: Materials, Device Physics, and Manufacturing Technologies*, ed. C. Brabec, V. Dyakonov and U. Scherf, Wiley-VCH, Weinheim, Germany, 2008.
- L. Dou, J. You, J. Yang, C.-C. Chen, Y. He, S. Murase, T. Moriarty, K. Emery, G. Li and Y. Yang, *Nat. Photonics*, 2012, **6**, 180–185.
- (a) S. Berson, R. D. Bettignies, S. Bailly and S. Guillerez, *Adv. Funct. Mater.*, 2007, **17**, 1377–1384; (b) C. W. Chu, H. Yang, W. J. Hou, J. Huang, G. Li and Y. Yang, *Appl. Phys. Lett.*, 2008, **92**, 103306.
- (a) J. Zhou, X. Wan, Y. Liu, Y. Zuo, Z. Li, G. He, G. Long, W. Ni, C. Li, X. Su and Y. Chen, *J. Am. Chem. Soc.*, 2012, **134**, 16345–16351; (b) T. S. van der Poll, J. A. Love, T.-Q. Nguyen and G. C. Bazan, *Adv. Mater.*, 2012, **24**, 3646–3649; (c) A. K. K. Kyaw, D. H. Wang, D. Wynands, J. Zhang, T.-Q. Nguyen, G. C. Bazan and A. J. Heeger, *Nano Lett.*, 2013, **13**, 3796–3801.
- Heliatek GmbH; press release on <http://www.heliatek.com>.
- G. Yu, J. Gao, J. C. Hummelen, F. Wudl and A. J. Heeger, *Science*, 1995, **270**, 1789–1791.
- (a) R. Fitzner, E. Reinold, A. Mishra, E. Mena-Osteritz, H. Ziehlke, C. Körner, K. Leo, M. Riede, M. Weil, O. Tsaryova, A. Weiss, C. Urich, M. Pfeiffer and P. Bäuerle, *Adv. Funct. Mater.*, 2011, **21**, 897–910; (b) R. Fitzner, E. Mena-Osteritz, A. Mishra, G. Schulz, E. Reinold, M. Weil, C. Körner, H. Ziehlke, C. Elschner, K. Leo, M. Riede, M. Pfeiffer, C. Urich and P. Bäuerle, *J. Am. Chem. Soc.*, 2012, **134**, 11064–11067.
- B. Walker, A. B. Tamayo, X.-D. Dang, P. Zalar, J. H. Seo, A. Garcia, M. Tantiwiwat and T.-Q. Nguyen, *Adv. Funct. Mater.*, 2009, **19**, 3063–3069.
- T. Bura, N. Leclerc, R. Bechara, P. Lévêque, T. Heiser and R. Ziessel, *Adv. Energy Mater.*, 2013, **3**, 1118–1124.
- (a) G. Wei, S. Wang, K. Sun, M. E. Thompson and S. R. Forrest, *Adv. Eng. Mater.*, 2011, **2**, 184–187; (b) A. Ajayaghosh, *Acc. Chem. Res.*, 2005, **38**, 449–459.
- W. W. H. Wong, T. B. Singh, D. Vak, W. Pisula, C. Yan, X. Feng, E. L. Williams, K. L. Chan, Q. Mao, D. J. Jones, C.-Q. Ma, K. Müllen, P. Bäuerle and A. B. Holmes, *Adv. Funct. Mater.*, 2010, **20**, 927–938.
- N. M. Kronenberg, M. Deppisch, F. Würthner, H. W. A. Ladermann, K. Deing and K. Meerholz, *Chem. Commun.*, 2008, 6489–6491.

- 14 H. Bürkstümmer, E. V. Tulyakova, M. Deppisch, M. R. Lenze, N. M. Kronenberg, M. Gsänger, M. Stolte, K. Meerholz and F. Würthner, *Angew. Chem., Int. Ed.*, 2011, **45**, 11628–11632.
- 15 Y. Sun, G. C. Welch, W. L. Leong, C. J. Takacs, G. C. Bazan and A. J. Heeger, *Nat. Mater.*, 2011, **11**, 44–48.
- 16 J. Zhou, X. Wan, Y. Liu, Y. Zuo, Z. Li, G. He, G. Long, W. Ni, C. Li, X. Su and Y. Chen, *J. Am. Chem. Soc.*, 2012, **134**, 16345–16351.
- 17 Y.-H. Chen, L.-Y. Lin, C.-T. Lun, F. Lin, Z.-Y. Huang, H.-W. Lin, P.-H. Wang, Y.-H. Liu, K.-T. Wong, J. Wen, D. J. Miller and S. B. Darling, *J. Am. Chem. Soc.*, 2012, **134**, 13616–13623.
- 18 (a) T. Rousseau, A. Cravino, T. Bura, G. Ulrich, R. Ziessel and J. Roncali, *Chem. Commun.*, 2009, 1673–1675; (b) T. Rousseau, A. Cravino, T. Bura, G. Ulrich, R. Ziessel and J. Roncali, *J. Mater. Chem.*, 2009, **19**, 2298–2300; (c) T. Rousseau, A. Cravino, E. Ripaud, P. Leriche, S. Rihn, A. De Nicola, R. Ziessel and J. Roncali, *Chem. Commun.*, 2010, **46**, 5082–5084.
- 19 T. Bura, N. Leclerc, S. Fall, P. Lévêque, T. Heiser, P. Retailleau, S. Rihn, A. Mirloup and R. Ziessel, *J. Am. Chem. Soc.*, 2012, **134**, 17404–17407.
- 20 (a) B. S. Kim, B. Ma, V. R. Donuru, H. Liu and J. M. J. Fréchet, *Chem. Commun.*, 2010, **46**, 4148; (b) T. Bura, N. Leclerc, S. Fall, P. Lévêque, T. Heiser and R. Ziessel, *Org. Lett.*, 2011, **13**, 6030–6033; (c) H.-Y. Lin, W.-C. Huang, H.-H. Chou, C.-Y. Hsu, J. T. Lin and H. W. Lin, *Chem. Commun.*, 2012, **48**, 8913–8915.
- 21 (a) S. Hattori, K. Ohkubo, Y. Urano, H. Sunahara, T. Nagano, Y. Wada, N. V. Tkachenko, H. Lemmetyinen and S. Fukuzumi, *J. Phys. Chem. B*, 2005, **109**, 15368–15375; (b) S. Erten-Ela, M. D. Yilmaz, B. Icli, Y. Dede, S. Icli and E. U. Akkaya, *Org. Lett.*, 2008, **10**, 3299–3302; (c) D. Kumaresan, R. P. Thummel, T. Bura, G. Ulrich and R. Ziessel, *Chem.–Eur. J.*, 2009, **15**, 6335–6339; (d) S. Kolemen, Y. Cakmak, S. Erten-Ela, Y. Altay, J. Brendel, M. Thelakkat and E. U. Akkaya, *Org. Lett.*, 2010, **12**, 3812–3815.
- 22 (a) R. Ziessel, G. Ulrich and A. Harriman, *New J. Chem.*, 2007, **31**, 496–501; (b) G. Ulrich, R. Ziessel and A. Harriman, *Angew. Chem., Int. Ed.*, 2008, **47**, 1184–1201.
- 23 J. H. Olivier, J. Barbera, E. Bahaidarah, A. Harriman and R. Ziessel, *J. Am. Chem. Soc.*, 2012, **134**, 6100–6103.
- 24 G. Ulrich, S. Goeb, A. De Nicola, P. Retailleau and R. Ziessel, *Synlett*, 2007, 1517–1520.
- 25 D. R. Coulson, L. C. Satek and S. O. Grim, *Inorg. Synth.*, 1972, **13**, 121–124.
- 26 G. Qian, B. Dai, M. Luo, D. Yu, J. Zhan, Z. Zhang, D. Ma and Z. Y. Wang, *Chem. Mater.*, 2008, **20**, 6208–6216.
- 27 A. Leliège, C.-H. Le Régent, M. Allain, P. Blanchard and J. Roncali, *Chem. Commun.*, 2012, **48**, 8907–8909.
- 28 CrystalClear-SM Expert 2.0 r4 (Rigaku, 2009).
- 29 G. M. Sheldrick, *Acta Crystallogr., Sect. A: Found. Crystallogr.*, 2008, **64**, 112–122; R. Welter, *Acta Crystallogr.*, 2006, **A62**, S252–S254.
- 30 A. L. Spek, *J. Appl. Crystallogr.*, 2003, **36**, 7–13.
- 31 M. N. Burnett and K. J. Carroll, Oak Ridge National Laboratory Report ORNL-6895, 1996.
- 32 C. F. Macrae, P. R. Edgington, P. McCabe, E. Pidcock, G. P. Shields, R. Taylor, M. Towler and J. van de Streek, *J. Appl. Crystallogr.*, 2006, **39**, 453–457.
- 33 A. N. Sobolev, V. K. Belsky, I. P. Romm, N. Yu. F. Chernikova and E. N. Guryanova, *Acta Crystallogr.*, 1985, **C41**, 967–971.
- 34 R. Ziessel, T. Bura and J.-H. Olivier, *Synlett*, 2010, 2304–2310.
- 35 R. Ziessel, G. Ulrich, A. Harriman, M. A. H. Alamiry, B. Stewart and P. Retailleau, *Chem.–Eur. J.*, 2009, **15**, 1359–1369.
- 36 A. Mirloup and R. Ziessel, *Tetrahedron Lett.*, 2013, **54**, 4456–4462.
- 37 A. Nano, R. Ziessel, P. Stachelek and A. Harriman, *Chem.–Eur. J.*, 2013, **19**, 13528–13537.
- 38 R. Ziessel, L. Bonardi, P. Retailleau and G. Ulrich, *J. Org. Chem.*, 2006, **71**, 3093–3102.